Spatial-temporal analysis of road raveling and its correlation with traffic flow characteristics

Wang, Z.; Krishnakumari, P.; Anupam, K.; Lint, J. W. C. van; Erkens, S. M. J. G.

DOI
10.1109/ITSC55140.2022.9922580

Publication date
2022

Document Version
Final published version

Published in
Proceedings of the 2022 IEEE 25th International Conference on Intelligent Transportation Systems (ITSC)

2022 IEEE 25th International Conference on Intelligent Transportation Systems (ITSC)
October 8-12, 2022, Macau, China

Spatial-temporal analysis of road raveling and its correlation with traffic flow characteristics

Z. Wang[1,2], P. Krishnakumari[1], K. Anupam[1], J. W. C. van Lint[1], and S. M. J. G. Erkens[1]

Abstract— **Understanding the relationship between pavement raveling and traffic characteristics is important to pavement management and maintenance planning. In this work, we propose a framework to empirically quantify this relationship. It consists of an alignment method to tackle the inconsistent spatial-temporal scales of the raveling and traffic measurements and we propose spatial-temporal maps to qualitatively analyze and compare the data. A non-parametric correlation is done on the aligned raveling and traffic flow data. This framework is applied to five study areas in the Dutch highway network. The correlation analysis of the study areas provides empirical evidence to a commonly held theory that traffic flow has effects on raveling. Categorizing the correlation by lanes indicates that the raveling is homogeneous in the through or auxiliary lanes, and the severe raveled sections are parallel to the road discontinuity, suggesting the potential effect of mandatory lane changing on raveling development. The proposed framework can be employed in empirical raveling models that predict raveling based on traffic and other factors.**

I. INTRODUCTION

Pavement health is crucial for smooth traffic operations. Several indicators of distress (external indications of pavement defects or deterioration [1]) are used to assess this health. Raveling, the aggregate loss caused by traffic load, weather conditions, or other reasons [2], is becoming a common form of distress during the recent years. This is mainly because of the use of porous asphalt for pavements, which can reduce noise [3] but is prone to raveling. Raveling contributes to 90% of the surface damage on porous asphalt [4]. It is important to understand the raveling phenomenon and its characteristics; especially for road agencies who manage the porous asphalt pavement.

Many models have been developed to understand the reasons for raveling formation and development. They can be broadly classified into mechanics and empirical models [5]. The first is based on physical theories of the structural behavior of pavement, typically explored using laboratory data. Empirical models employ statistical analysis of the deterioration progress based on field observation data. From mechanics analyses, it appears that raveling is caused mainly by force, especially tensile and shear force [2][6]. Several factors make this force critical, such as inadequate mix design [6][7], poor production quality [7], inappropriate transportation conditions, bad construction quality, traffic [2][8], extreme weather conditions [6], and fatigue [2][6]. Many empirical models indicate that factors such as material types [9][10][11], material production [11], construction[9][11][12], climate [10][11], winter treatment [13], traffic [9]-[14] and service time [9] have an influence on raveling. Traffic is thus found to be a significant factor for raveling using both mechanics and empirical models.

Mechanics models suggest that traffic affects raveling via force, stress, strain, modulus, and fatigue. The movement of wheels generates shear force, causing stone loss from the road surface [8]. Since raveling is the loss of aggregate that occurs at the stone-on-stone contact regions [6], it is important to identify those traffic characteristics that generate the force to break the stone-on-stone contact, such as critical shear force. Different studies show that heavy vehicles [15][16] and overloaded vehicles [17] cause significant shear force. Although mechanics models have strong theoretical underpinnings, they rely on parameters that are hard to be measured in practice [5].

Empirical studies analyze the correlation between raveling and multiple factors—some of which are related to traffic; and estimate general regression or classification models that encode these correlations. However, such studies typically result in localized models [5] that may not generalize well to other conditions. For example, the Highway Development and Management model (HDM) [5][18][19] is calibrated for applying to cases in Ethiopia [9], India [12], Chile [20], and America [21]. Researchers in Sweden and Denmark [13] and the Netherlands [22] have developed raveling models based on logistic regression. Many recent articles employ machine learning for developing raveling models, such as artificial neural network [10][14], support vector regression [10][22], regression trees [10], rough set theory [10], k-nearest neighbors [22], and random forest [22]. There is no consensus on which is the best technique for building a raveling model due to the wide range of factors that must be considered, and insufficient accuracy of field data [23].

The research aim is to quantify the effect of traffic on raveling using empirical models. Despite the limitations of empirical models, the current trend in pavement management of transforming from visual inspection to automatic measurement [23] promises a large amount of field data to become available for extended calibration and validation of such models. The main challenge for developing a good empirical raveling model is that (a combination of) many factors cause pavement deterioration, some of which are correlated with each other. Disentangling these correlations and understanding their relationships can lead to better models. To address this explicitly, we conduct the empirical analysis on traffic effects on raveling while controlling for other factors through study area selection.

[1] Faculty of Civil Engineering and Geosciences, Delft University of Technology, 2628 CN Delft, Netherlands
[2] Z.wang-17@tudelft.nl

2022 IEEE 25th International Conference on Intelligent Transportation Systems (ITSC) | 978-1-6654-6880-0/22/$31.00 ©2022 IEEE | DOI: 10.1109/ITSC55140.2022.9922580

Another challenge we explicitly address is the fundamental spatial-temporal misalignment of raveling and traffic data. This misalignment relates particularly to the large difference in temporal resolution. Raveling is a long-term process in which the deterioration is measured in terms of months to years whereas traffic is a dynamic process that is measured sometimes to the second. Traditional pavement performance models employ the Average Annual Daily Traffic (AADT) to represent traffic state, and typically neglect the traffic variation across different lanes. Therefore, in this paper we propose a systematic spatial-temporal aggregation mechanism for traffic and raveling data in order to conduct correlation between them.

This research is on the interface between the pavement engineering and traffic engineering domains. It is structured as follows: the spatial-temporal aggregation mechanism and the analytical model for correlation analysis is proposed in Sec. II, a Dutch case study is introduced in Sec.III to which our framework is applied, the main results are elaborated and discussed in Sec. IV and finally, the conclusions are presented at the end of the paper.

II. METHODOLOGY

Physical quantities with causal relationships are observed to have strong data correlation, thus this paper investigates the correlation between traffic characteristics and raveling. The challenge is that traffic and raveling have different measurement dimensions. Due to the design of loop detectors (widely used traffic data collection systems), traffic data is point-based, i.e. data is collected when vehicles cross a measurement spot. On the other hand, raveling, defined as the amount of the dislodged aggregates from an area, is area-based data. Another problem is that traffic and raveling data have significantly different spatial and temporal resolutions. Usually, traffic temporal resolution is higher than raveling, but traffic spatial resolution is lower than raveling.

The correlation analysis takes in two sets of inputs: traffic flow and raveling. Point-based or link-based traffic flow defines q. When q is point-based, it refers to the number of vehicles passing a location x from time t to time $t + \Delta t$; and when q is link-based, it refers to the number of vehicles traversing a trajectory jk from time t to time $t + \Delta t$. Link-based or area-based raveling defines r. When r is area-based, it is the amount of aggregates dislodged from area a from time t to time $t + \Delta t$; when r is link-based, it is the amount of aggregates dislodged from an 1-meter wide area between locations m and n from t to $t + \Delta t$. Clearly, the analysis requires an identical dimension and a consistent attribute resolution. Therefore, this paper presents the spatial and temporal alignment models, as a part of the framework for correlation analysis in Fig. 1. It also provides traffic flow and raveling state estimation models to tackle the mismatch between point-based, area-based and link-based measurements, which convert q and r into link-based attributes. The well-known Adaptive Smoothing Method (ASM) [24] is used to estimate traffic flow. Moreover, four parameters of spatial and temporal resolutions of traffic and raveling are computed within the framework. Data collection systems and/or ASM determine the traffic temporal resolution t^q. The temporal resolution of raveling t^r, the spatial resolution of traffic x^q and raveling x^r are defined as the time between the first service day (after a construction or a maintenance) and the inspection day of r, the locations j and k of the link-based q, and the locations m and n of the link-based r respectively.

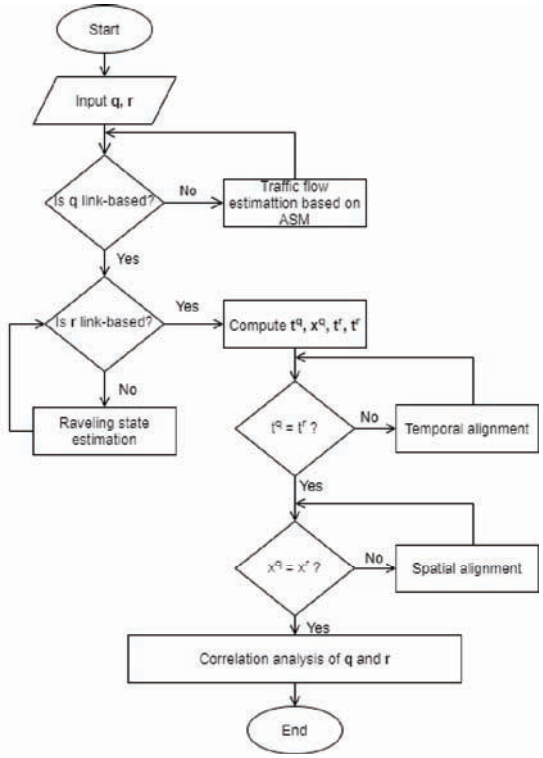

Fig. 1: Framework for raveling and traffic flow correlation analysis

A. Traffic flow estimation based on ASM

Treiber and Helbing [24] introduced ASM to obtain continuous traffic variables (e.g. traffic flow) in both space and time from station data. This method solves the aforementioned problem of the mismatched traffic and raveling dimensions, especially extrapolating point-based data to link-based. ASM uses a non-linear spatial-temporal lowpass filter to convert discrete vehicle counts into a smooth spatial-temporal function of traffic flow as Eq. 1 from [24] indicates. This filter is formulated according to the traffic flow theory that the wave propagates upstream at a constant speed in the congested traffic, and downstream at the free-flow speed in the free traffic.

$$\begin{aligned}\dot{q}(x^q, t^q) =& \omega(\mathrm{q}^{cong}, \mathrm{q}^{free})\mathrm{q}^{cong}(x,t) \\ &+ (1-\omega(\mathrm{q}^{cong}, \mathrm{q}^{free}))\mathrm{q}^{free}(x,t)\end{aligned} \tag{1}$$

where $\dot{q}$ is the number of vehicles passing through a trajectory between locations x^q during the time t^q, ω is the filter, q^{cong} and q^{free} are the congested traffic flow and the free flow respectively, and x and t are the measurement locations

and the measurement time of the congested/free traffic flows. x^q is uniformly distributed, ranging from $x+\Delta x$, $x+2\Delta x$, $x+3\Delta x$, etc. t^q is also uniformly distributed, ranging from $t+\Delta t$, $t+2\Delta t$, $t+3\Delta t$, etc. Δx and Δt are the given parameters of the spatial resolution and the temporal resolution. x and t are determined by the measurement method. The filter $\omega \quad [0,1]$ depends on the speed of q and the speed parameters of the congested and free-flow traffic. Both q^{cong} and q^{free} are derived from the input data of q, the speed of q, and the speed parameters of the congested and free traffic state. After the computation of $\dot{q}$, the q is updated by $\dot{q}$, according to Fig. 1.

B. Raveling state estimation

Using the raveling state estimation, the area-based raveling is changed into the related link-based raveling. In Eq. 2, the link-based raveling of a given link is the quotient of all the area-based raveling on this link divided by the total width of the measured areas.

$$\dot{r}(x^r,t^r)=\frac{\sum^{y^r} r(x^r,y^r,t^r)}{\sum y^r} \tag{2}$$

where r is the amount of the dislodged aggregates from a measurement area during the time t^r, x^r and y^r are the locations and the width of the measurement area respectively, and $\dot{r}$ is the amount of the dislodged aggregates of 1-meter wide area during the time t^r. t^r, x^r and y^r are all determined by the measurement method of r. After the computation of $\dot{r}$, the r is updated by $\dot{r}$ according to Fig. 1.

C. Temporal alignment

Given that raveling and traffic data are link-based or have been transformed into link-based data, the next step is the spatial-temporal alignment. In this paper, we downsample the data to the lowest temporal resolution among the raveling and traffic. Downsampling/lower temporal resolution just requires aggregation, whereas upsampling/higher resolution data requires extrapolation or data collection system upgrades, which are not viable. The temporal alignment has two scenarios: (1) $\Delta t^r > \Delta t^q$, which means raveling has lower temporal resolution than traffic flow; (2) $\Delta t^r < \Delta t^q$, which means traffic flow has lower temporal resolution than raveling. In the first scenario, this temporal alignment model aggregates short-term flows into long-term flows. The second scenario is only theoretically possible. In practice, the raveling is measured every season or year whereas the traffic data collection systems upload data in seconds, minutes, hours or days. Thus, this paper introduces the temporal alignment only for the first scenario, where traffic has a higher temporal resolution than raveling.

The model aggregates the short-term traffic flows into a long-term flow at a given temporal resolution. The aggregated traffic flow is the sum of two parts in Eq. 3: the first is an aggregation of the traffic flows $\dot{q}$ during all the time t^q within the selected raveling temporal resolution t^r; and the second is the product of the average traffic flow $\bar{q}$ of a given period T and the time beyond observation during t^r. Eq. 4 formulates $\bar{q}$. The second part in Eq. 3 tackles the problems: (1) a pavement has accommodated traffic before the observation starts; (2) the measurement is vacant at some observation periods. It is highlighted that Eq. 3 is based on the assumption that the flow at the unmeasured time is equals to the average traffic flow $\bar{q}$ of the period T during the observation. According to Fig.1, after the computation of $\ddot{q}$, the q is updated by $\ddot{q}$.

$$\ddot{q}(x^q,t^r)=\sum_{t^q=t^q_{min}}^{min(t^q_{max},t^r)}\dot{q}(x^q,t^q)+\bar{q}(x^q)(t^r-\sum_{t^q_{min}}^{min(t^q_{max},t^r)}t^q) \tag{3}$$

$$\bar{q}(x^q)=\frac{\sum_{t^q=t^q_{min}}^{T}\dot{q}(x^q,t^q)}{\sum_{t^q=t^q_{min}}^{T}t^q},\ T \quad (t^q_{min},t^q_{max}] \tag{4}$$

where $\ddot{q}$ is the number of vehicles traversing between locations x^q during the raveling temporal resolution t^r, $\dot{q}$ is the number of vehicles traversing between locations x^q during the time t^q, t^q_{min} and t^q_{max} are the earliest and last measurements of t^q, and $\bar{q}$ is the average traffic flow traversing between locations x^q of a given period T within the entire observation time from t^q_{min} to t^q_{max}.

Because we have selected the raveling temporal resolution for the proposed model, the temporal alignment is not required for the raveling attribute. The values of $\dot{r}$ are assigned to $\ddot{r}$ in Eq.5.

$$\ddot{r}(x^t,t^r)=\dot{r}(x^t,t^r) \tag{5}$$

where $\ddot{r}$ is the amount of the dislodged aggregates of an 1-meter width area between locations x^r during time t^r, and the same as $\dot{r}$.

D. Spatial alignment

Aligning traffic with raveling in the same spatial scale requires a similar aggregation operation as in the temporal alignment. The aligned spatial scale is determined as the larger scale among traffic and raveling. This means that the alignment model converts the high-resolution attribute into the low-resolution attribute. Two scenarios are: (1) $\Delta x^r > \Delta x^q$, the length of mn is longer than jk, which means raveling spatial resolution is lower than traffic flow; (2) $\Delta x^r < \Delta x^q$, the length of mn is smaller than jk that indicates traffic has lower spatial resolution than raveling. In the first scenario, we estimate the traffic flow of the link mn by the traffic flows of the small links jk within mn. In the second scenario, we estimate the raveling of the link jk by the raveling of the small links mn within jk.

We use statistics for the spatial alignment. We find the p-th percentile of a variable v from a sample V. For example, the 75th percentile of v is the value that 75% of the items from the sample V are smaller or equal to. The v's percentile is a function of the percentile p and the sample V namely $v=f(V,p)$. Dependent on the scenarios, the spatial alignment computes the traffic flow or raveling percentiles. When the time intervals Δx^r of raveling $\ddot{r}$ is longer than that of traffic

flow Δx^q, Eq.6 is used. When the time intervals Δx^r of raveling $\ddot{r}$ is shorter than that of traffic flow Δx^q, Eq.7 is used. According to Fig.1, the q or r is updated by $\ddot{\ddot{q}}$ or $\ddot{\ddot{r}}$ respectively, after the computation of $\ddot{\ddot{q}}$ or $\ddot{\ddot{r}}$.

if $\Delta x^r > \Delta x^q$,

$$\ddot{\ddot{q}}(x^r, t^r) = f(Q, p)\ (\ddot{q}(x^q, t^r) \quad Q, x^q \quad x^r) \tag{6}$$

else if $\Delta x^r < \Delta x^q$,

$$\ddot{\ddot{r}}(x^q, t^r) = f(R, p)\ (\ddot{r}(x^r, t^r) \quad R, x^r \quad x^q) \tag{7}$$

where $\ddot{\ddot{q}}$ is the p-th percentile from the sample Q that consists of the traffic flows $\ddot{q}$ passing though all the trajectories between locations x^q within the locations x^r, and $\ddot{\ddot{r}}$ is the p-th percentile from the sample R that consists of all the link-based raveling $\ddot{r}$ between the locations x^r within x^q. p is a given parameter of the percentile.

E. Correlation analysis

Parametric or non-parametric statistics are used to calculate correlation coefficients between variables. When the data is (nearly) normally distributed, parametric statistics are used. Otherwise, non-parametric statistics are used. A normality test is performed initially, with the null hypothesis that the data is normally distributed. The variable is normally distributed when the p-value is greater than the significant level of 5%.

We use Pearson's linear correlation coefficient ρ in Eq. 8 for the parametric statistics, and Spearman's ρ for the non-parametric statistics. Spearman's ρ is formulated like the Pearson correlation coefficient in Eq. 8 but based on the ranking of data in the sets.

$$\rho(x, y) = \frac{\sum_{i=1}^{n}(x_i - \hat{x})(y_i - \hat{y})}{\sum_{i=1}^{n}(x_i - \hat{x})^2 \sum_{i=1}^{n}(y_i - \hat{y})^2} \tag{8}$$

where ρ is the correlation coefficient of data sets x and y, x_i and $\hat{x}$ are the data and the average of x, y_i and $\hat{y}$ are the data and the average of y, i is the sequence number of the data in the sets x or y, and n is the number of data in x or y. According to the algorithm in Fig. 1, x and y represent either $\ddot{q}(x^q, t^r)$ and $\ddot{\ddot{r}}(x^q, t^r)$ or $\ddot{q}(x^q, t^r)$ and $\ddot{\ddot{r}}(x^q, t^r)$. Because the spatial-temporal resolutions x^q, x^r, t^r are irrelevant to the computation of ρ, the one-dimension x and y can represent the spatial-temporal dependent variables.

In addition, the p-value is calculated to see if the correlation between raveling and traffic is statistically significant. Two variables are uncorrelated, which is what the null hypothesis test presupposes. They are correlated when the p-value is less than the significant interval (5%).

III. EXPERIMENTAL SETUP

A. Data

Defined by the supporting inspection system, raveling is measured by scanning the road surface and generating 3D pictures with high-speed laser triangulation. When the surface pictures show cavities, it is assumed that this indicates the aggregates being lost. The coin algorithm is employed, which indicates a lost aggregate when a cavity is equal to or larger than a specific coin size. The export of the inspection system is given as the ratio of the sum area size of the lost aggregates to the measurement area size. The coin size has three candidate values: (1) the diameter of 6 mm and the height of 2 mm; (2) the diameter and height of 3 mm; and (3) the diameter of 1.5 mm and the height of 3 mm. The inspection system also determines the picture resolution and position. The picture is 1 meter by 1 meter. For instance, a 3.4-meter wide lane can have three parallel lateral photos taken. In practice, two photos of the left and right wheel trajectories are taken. The left wheel trajectory is the range of 1 meter from the road marking on the left side towards the center of the lane. The right wheel trajectory is the range of 1 meter from the road marking on the right side towards the center of the lane. A section has six values of the raveling measurement, according to three coin sizes and left/right trajectory. Along with raveling data, the data of construction and maintenance dates are also provided.

Traffic data are collected by loop detectors. These detectors are attached to the roadway coating and count the number of passing vehicles and their corresponding speeds in (near) real-time. The traffic flow and speed are collected every minute and stored consecutively in the database.

These datasets have been cleaned for this study. Some of the problems that were addressed and tackled are: (1) databases are notorious for containing mostly null values (which are internally often encoded as a series of space characters); (2) duplicate data; (3) outliers; and (4) different data collection systems with different Geographical Information Systems (GISs).

B. Study areas

To obtain meaningful correlations, we selected study areas by controlling as many external factors as possible. The selection criteria for the study areas include: (1) the surface material is porous asphalt, which is sensitive to road damage due to raveling; (2) the pavement configuration had no change during the observation period between 2012 and 2020; (3) the selected areas have reliable measurements for both traffic and pavement condition for the selected periods; and (4) each study area is as long as two kilometers, within which the environmental conditions are expected to be the same. Although a few sections meet the selection criteria, due to limited data storage and computational power, this study only explores five study areas. These areas are located at four Dutch motorways as shown in Fig. 2.

IV. RESULTS AND DISCUSSION

This section presents the spatial-temporal characteristics of raveling and traffic and the outputs of the different steps in the framework. The method is applied to the field measurement data from the five study areas between 2012 and 2020. In order to compare raveling and traffic and capture the spatial and temporal dynamics of these data sources in a single visualization, we used spatial-temporal maps where the 'x-axis' can represent either time or geographical

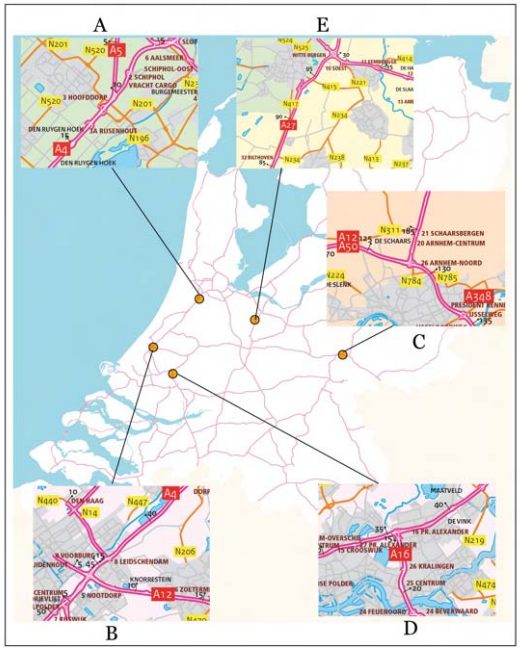

Fig. 2: A map of Dutch highway network in which the five study areas are highlighted

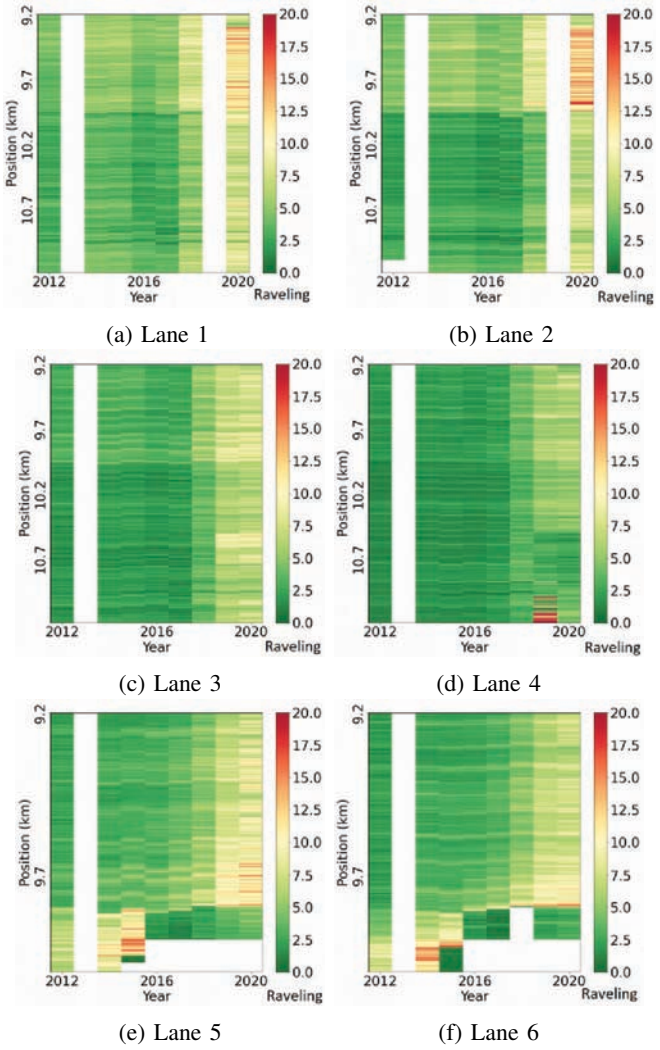

(a) Lane 1 (b) Lane 2

(c) Lane 3 (d) Lane 4

(e) Lane 5 (f) Lane 6

Fig. 3: Raveling homogeneity and heterogeneity of the through and auxiliary lanes for study area A

lane, the 'y-axis' represents the location and the color can represent either traffic or raveling variables.

First, we explore the spatial-temporal characteristics of raveling and traffic data independently. Raveling was found to be spatially homogeneous in the through lanes in terms of quantities and increments. According to the eight-year observation of lanes 1 and 2 (both are through lanes), the mean and standard deviations of raveling quantities in the study area A lane 1 are 4.90 and 2.39 respectively, and those of its lane 2 are 4.58 and 2.77. The cosine similarity between them is 0.96, indicating a strong resemblance between the two lanes. As for the study areas B, C, D and E, the cosine similarity of the two through lanes has the values of 0.70, 0.88, 0.81 and 0.76 respectively. The value close to 1 indicates a strong similarity between two variables. The raveling homogeneity exists also in the auxiliary lanes. For example, the mean and the standard deviation of raveling in the study area A are 5.04 and 2.90 for one deceleration lane, and 4.50 and 2.68 for another. Their cosine similarity is 0.96. The raveling of the through and auxiliary lanes is relatively heterogeneous. The cosine similarity is 0.89 between lane 1(left through lane) and lane 5 (left auxiliary lane) of study area A. Besides, in the cases of B and D (the study areas C and E do not contain any auxiliary lane), the values of the cosine similarity are 0.61 and 0.80 respectively. The lane homogeneity and heterogeneity are apparent in the graphical analysis results as well. Fig 3 depicts the 8-year raveling of all the lanes in study area A. The patterns of the auxiliary lanes (lanes 5 and 6) differ from the through lanes (lanes 1, 2, 3 and 4), but bear a clear resemblance to each other.

The data exploration of the study areas shows that in a through lane, the heterogeneous raveled areas are located parallel to the deceleration and acceleration lanes. This finding is supported by the graphical results of the raveling spatial distributions, one example of which as Fig. 4 plots the study area A. It shows the raveled areas (colored red) at the upstream where the deceleration lanes exist. The downstream where an acceleration lane occurs is too short to discern a heterogeneous raveling pattern, but where the acceleration lane appears in study area B, the heterogeneous raveled regions of the through lanes have been observed.

Raveling initial spatial scales are determined by data collection systems, which are 1-meter areas in this case. To explore the effects of the spatial scales on estimating raveling condition and progression, this study computes the aggregated quantities of the spatial scales of 5-meter, 10-meter, 20-meter, 100-meter, and 200-meter. Fig. 5 shows four of these scales for the study area D lane 1. When the spatial scales are bigger than 20 meters, the data is aligned better than that of a smaller scale. The difference in locations from each year's measurement is approximately longer than

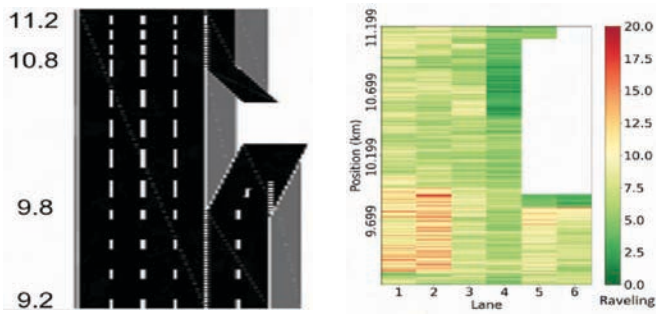

(a) Road configuration (b) Raveling of 2020

Fig. 4: Raveling spatial distribution of the study area A

20 meters. Aggregating raveling into larger spatial scales is beneficial to raveling progression detection but it neglects localized patterns. Spatial aggregation is an effective solution to the problem of unaligned annual raveling data because the inspection vehicles provide the inaccurate measurement coordinates. This comparison is considered in the spatial scale selection in the proposed spatial alignment model.

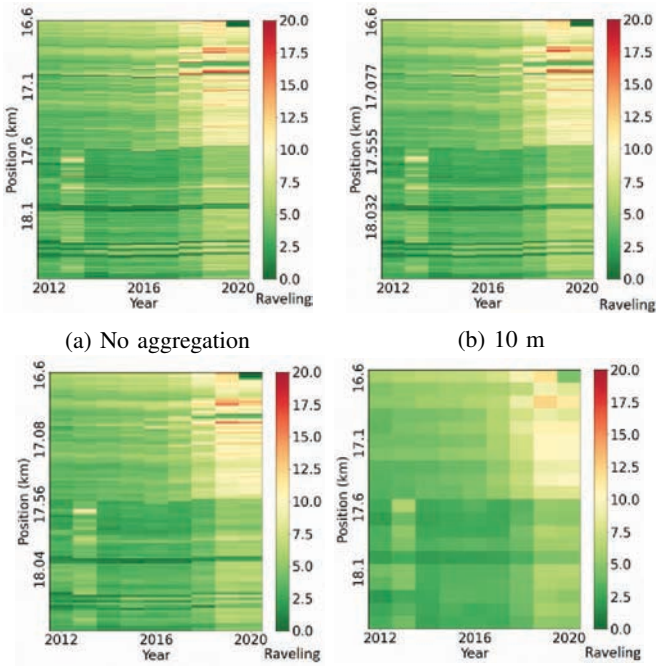

(a) No aggregation (b) 10 m

(c) 20 m (d) 100 m

Fig. 5: Different spatial-scale raveling based on the study area D lane 1 - no aggregation, 10m, 20m, 100m, 200m

In order to transform the area-based raveling data to link-based data, raveling state estimation is applied. The average of all measurements of a given lane in the transverse direction is assigned as the link raveling quantity and is dependent on the link length. In this work, the measurement resolution is 1-meter length and the link-level raveling is the average of the percentages of the lost aggregate at the left-wheel and right-wheel trajectories. The distributions of the link-based raveling quantities in the five study areas are positively skewed and leptokurtic. The skewness of the study areas A to E are 2.16, 4.07, 1.18, 1.76 and 4.26 respectively, while that of the input data are 5.29, 4.24, 1.24, 1.95 and 6.21 respectively. The study areas A to E have the kurtosis (according to Fisher's definition) of the link-based raveling quantities as 15, 21, 2, 7 and 25, which are 93, 25, 2, 8 and 55 based on the inputs. Moreover, the raveling state estimation is not an interpolation method, and hence, the locations that lack data such as lane 1 of the study area A in 2013 and 2019 (the blanks in Fig. 3) have no values from this step.

There is also heterogeneity in traffic flow dynamics between the lanes as well. Aggregating the traffic data daily, weekly, monthly and annually on a road that has two through lanes, the right through lane accommodates more traffic than the left one. For example, in the study area C, the left though lanes had an average daily traffic flow of 403 veh/h in 2012; and the right one had 603 veh/h. On a road with more than two through lanes, the right lanes have higher flows than the left through lanes apart from the most right one. For example, in the study area A, lanes 1 to 4 accommodated 11%, 24%, 35% and 30% of through traffic in 2012 respectively. This relates to the Dutch right-to-drive policy. The preference for the second right through lanes is likely due to on- and off-ramp interference in the most right lanes.

The discrete traffic data (including the number of passing vehicles and the average of their speeds) are converted to the uniform traffic flow data by the ASM method. Fig. 6 shows the ASM output of study area A left lane for a single day in 2012. The result indicates that the ASM function smooths the data spatially and temporally. Such interpolation solves the problem of non-uniform spatial scales of the measurement due to the various densities of the loop detector networks. The output of traffic flow has a consistent spatial-temporal scale which is related to the ASM setting parameters. In this work, we use a spatial aggregation of 200 meters and a temporal aggregation of 1 minute.

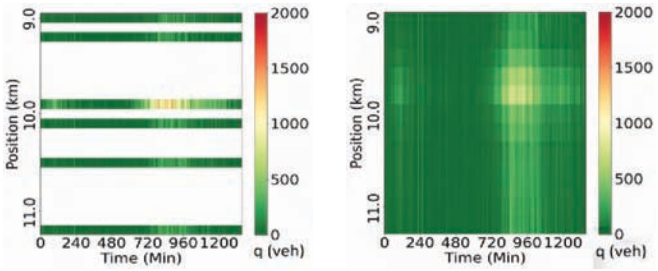

(a) Loop detector measurement (b) ASM result

Fig. 6: Hourly traffic flow of study area A on 1 January 2012

The ASM filtered traffic data is aggregated further in the temporal dimension to align with the highly aggregated raveling data. Fig. 7 shows the daily, weekly, and monthly aggregated traffic flows of study area A for 2012. The aggregation has hardly any influence on the spatial characteristics; high traffic flow is localized around 9.8km irrespective of the different temporal scales. The short-term dynamics are neglected as we are looking at long-term aggregation to

match with the multiple-year raveling data.

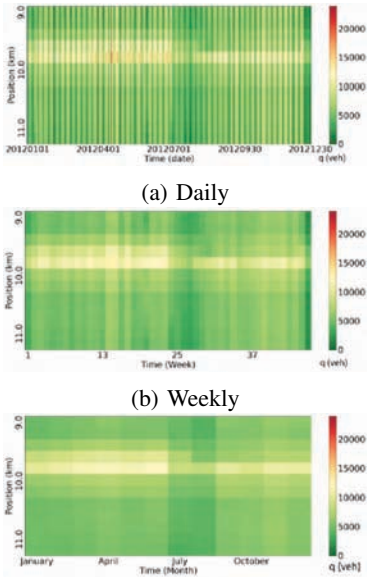

(a) Daily

(b) Weekly

(c) Monthly

Fig. 7: Aggregated traffic flow of study area A for 2012

Given the link-based estimated data from raveling and traffic, we can temporally align the data. The traffic temporal scale is 1 minute after ASM filtering, and is then aggregated into a day, a week, a month and a year's aggregates. The temporal scale of raveling is the service time (from the start of service after the last construction/maintenance to when raveling is measured). The temporal alignment parameter T should be longer than the traffic temporal scale and is recommended to be a period in the first observation year. In this work, the entire duration of 2012 is set as T.

For the spatial alignment of traffic and raveling, traffic has the higher spatial scale (100m) than raveling (1m). We use the traffic spatial unit for the alignment. The setting of the k-percentile has no significant influence on spatial alignment results in terms of data shapes and rankings. In this work, four settings of k-percentile (i.e., 25, 50, 75 and 90) are tested. The distributions of the five study areas are positively skewed and leptokurtic, just like the distribution of the inputs.

The spatially and temporally aligned traffic and raveling are used for the correlation analysis. Since the variables are not normally distributed, the non-parametric method is applied. The coefficients of the correlation analysis with their corresponding p-values are given in Tab. I. A value of the coefficient close to one indicates a strong correlation. When the p-values are less than the significance level (5%), the null hypothesis is rejected. According to the positive correlation coefficients, the more traffic flow a lane serves, the more severe the raveled condition is. Given the p-values, raveling and traffic are correlated. However, the correlation is not statistically significant without the categorization by lanes. The correlation coefficients of the five study areas are -0.04, 0.06, 0.40, 0.49 and 0.16, and the p-values are larger than the confidence (5%) for study areas A, B and D. This suggests the importance of lane and/or road topology in the estimation of raveling progression and in the raveling model.

Fig. 8 shows a detailed scatterplot of raveling and traffic flow per lane in the study areas. Linear regression is used to fit the data to generalize the raveling propensity with traffic flow increments. In the study areas A, B, C and D, the lines indicating lane 1 are steeper than those for other lanes, showing that raveling develops faster with similar traffic increments on the left lane. Due to the unbalanced data (only 6 points where traffic flow ranges from 6.5E7 to 1E8) in study area E, the slope of the fitted line is biased by the outliers. In addition, linear regression is not the best method to fit raveling and traffic. Based on Fig. 8, log or quadratic polynomial model with an upward opening seems to fit better. The quadratic polynomial has the characteristics that the dependent and independent variables are negatively correlated before the vertex and positively correlated after the vertex. In this case, the outliers exist at the early stage with moderate or severe raveling. The damage is expected to be attributed to construction quality rather than traffic flows.

Moreover, raveling rates on lane 2 are faster than lanes 3 and 4 in the four-through lane roadways (i.e. A and B). Given that the majority of traffic flows on a highway with four through lanes are on lane 3 and 4, and lane 1 accommodates the least, low-flow roads ravel faster than high-flow roads. It does not meet the expectation that the higher the traffic flow, the faster the raveling is developing. It is highlighted that the left lanes are usually used as the taking-over lanes, possibly causing the critical shear force to dislodge the aggregates, but this possibility can not be considered into the correlation analysis of traffic flow and raveling. Moreover, Henning and Roux [25] presented the same finding based on their study of New Zealand.

V. CONCLUSIONS

In this study, we quantified the relationship between raveling and traffic flow. To achieve this, several challenges need to be addressed. Even though traffic and raveling influence each other, they are measured at different spatial and temporal resolutions. Therefore, we needed to have a shared spatial-temporal aggregation for the raveling and traffic data. We used estimation methods and proposed alignment mechanisms to achieve this. We also proposed using spatial-temporal maps to visually represent the long term dynamics of both raveling and traffic concisely for qualitative analysis and comparison studies. The framework was applied to five carefully selected case study areas, trying to control for other external and data factors. A non-parametric correlation analysis was conducted for these areas. The results show that traffic and raveling are correlated to each other but only if categorized by lanes. Thus, road topology plays a significant role in this correlation.

There are various limitations to this study. Some of the limitations are related to data availability and completeness of raveling data. The spatial inaccuracies during the inspection and holes in the data add artifacts that could bias the analysis. In this work, we only considered traffic

TABLE I: Correlation coefficients of study areas

	Lane 1		Lane 2		Lane 3		Lane 4		Lane 5	
	ρ	p-value	ρ	p-value	ρ	p-value	ρ	p-value	ρ	p-value
A	0.25	<0.001	0.21	0.003	0.47	<0.001	0.43	<0.001	-	-
B	0.55	<0.001	0.20	0.04	-0.22	0.02	0.75	0.02	-	-
C	0.35	<0.001	0.44	<0.001	0.80	<0.001	-	-	-	-
D	0.83	<0.001	0.23	0.004	0.74	<0.001	0.80	<0.001	0.96	<0.001
E	0.18	0.17	0.45	<0.001	-	-	-	-	-	-

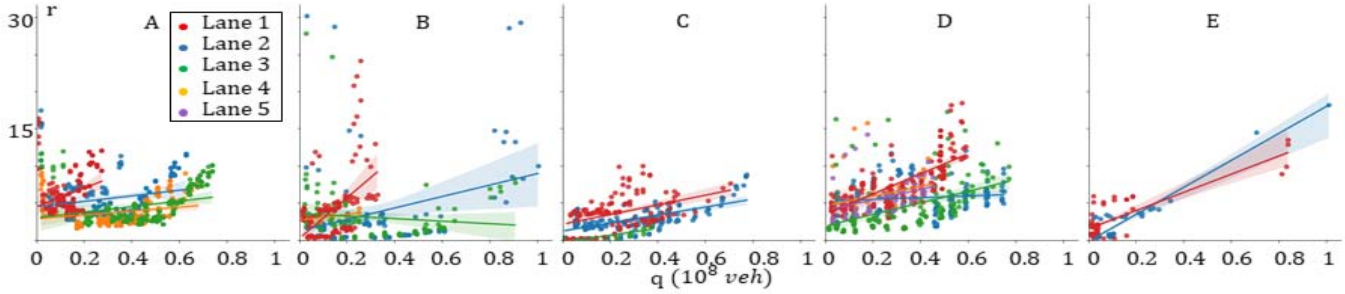

Fig. 8: Correlation between raveling and cumulative traffic flow per lane for study area A, B, C, D and E.

flow but there are many other traffic characteristics such as traffic mix and lane changing that can influence raveling. Moreover, we aggregated the traffic data to yearly averages and disregarded local traffic dynamics that might be relevant to extracting important relationships between these variables. These limitations open up many avenues for future research.

REFERENCES

[1] *ASTM Dictionary of Engineering Science & Technology*, 10th ed. ASTM International, 2005.

[2] H. Zhang, K. Anupam, A. Skarpas, C. Kasbergen, and S. Erkens, "Simple homogenization-based approach to predict raveling in porous asphalt," *Transportation Research Record*, vol. 2674, no. 12, pp. 263–277, 2020.

[3] J. C. Nicholls, "Drat–development of the ravelling test compendium of sites and the extent of ravelling," 2016.

[4] E. Vos and F. Bouman, "Oberflächeneigenschaften in den niederlanden–methoden und ziele," *Straße und Autobahn*, vol. 1, no. 2015, pp. 23–27, 2015.

[5] G. T. Rohde, "Modelling road deterioration and maintenance effects in hdm-4," *Pavement Strength in HDM-4 with FWDs*, 1995.

[6] L. Mo, M. Huurman, M. F. Woldekidan, S. Wu, and A. A. Molenaar, "Investigation into material optimization and development for improved ravelling resistant porous asphalt concrete," *Materials & Design*, vol. 31, no. 7, pp. 3194–3206, 2010.

[7] Q. You, N. Zheng, and J. Ma, "Study of ravelling failure on dense graded asphalt pavement," in *Proceedings of the Institution of Civil Engineers–Transport*, vol. 171, no. 3. Thomas Telford Ltd, 2018, pp. 146–155.

[8] J. De Visscher and A. Vanelstraete, "Ravelling by traffic: Performance testing and field validation," *International Journal of Pavement Research and Technology*, vol. 10, no. 1, pp. 54–61, 2017.

[9] S. Meskellie, "Evaluation of structural performance, deterioration and optimum maintenance strategies for asphalt roads," Master's thesis, Delft University of Technology, Civil Engineering and Geosciences, Delft University of Technology, the Netherlands, 2004.

[10] M. Miradi, "Knowledge discovery and pavement performance: Intelligent data mining," PhD thesis, Faculty of Civil Engineering and Geosciences, Delft University of Technology, 2009.

[11] T. Kuennen, "Loss of cover," *Better Roads*, vol. 83, no. 7, pp. 14–20, 2013.

[12] S. S. Jain, S. Aggarwal, and M. Parida, "Hdm-4 pavement deterioration models for indian national highway network," *Journal of Transportation Engineering*, vol. 131, no. 8, pp. 623–631, 2005.

[13] K. R. Opara, M. Skakuj, and M. Stöckner, "Factors affecting raveling of motorway pavements—a field experiment with new additives to the deicing brine," *Construction and Building Materials*, vol. 113, pp. 174–187, 2016.

[14] D. T. Thube, M. Parida, and S. S. Jain, "Application of artificial neural network (ann) for prediction of pavement deterioration for low volume roads in india," in *Research into Practice: 22nd ARRB ConferenceARRB*, 2006.

[15] S. S. Adlinge and A. Gupta, "Pavement deterioration and its causes," *International Journal of Innovative Research and Development*, vol. 2, no. 4, pp. 437–450, 2013.

[16] A. González, D. Cantero, and E. J. OBrien, "Dynamic increment for shear force due to heavy vehicles crossing a highway bridge," *Computers & Structures*, vol. 89, no. 23-24, pp. 2261–2272, 2011.

[17] H. U. Bae and M. G. Oliva, "Moment and shear load distribution factors for multigirder bridges subjected to overloads," *Journal of Bridge Engineering*, vol. 17, no. 3, pp. 519–527, 2012.

[18] T. Watanatada, C. G. Harral, W. D. Paterson, A. M. Dhareshwar, A. Bhandari, and K. Tsunokawa, "The highway design and maintenance standards model," *World Bank Highway Design and Maintenance Standards Series*, 1987.

[19] G. Morosiuk and M. Riley, "Modelling road deterioration and works effects in hdm-4," Tech. Rep., 2004.

[20] H. De Solminihac, H. S. Priscila, and S. T. Mauricio, "Calibration of performance models for surface treatment to chilean conditions: the hdm-4 case," *Transportation Research Record*, vol. 1819, no. 1, pp. 285–293, 2003.

[21] J. Li, S. T. Muench, J. Mahoney, G. White, L. Peirce, and N. Sivaneswaran, "Application of hdm-4 in the wsdot highway system," *Washington State Transportation Commission*, pp. 1–106, 2004.

[22] T. Van Loon, "Effect of environmental conditions on the longevity of thin noise-reducing asphalt top layers: A case study in the province of gelderland," Master's thesis, Geo-information science, Wageningen University Research, Wageningen, the Netherlands, 2018.

[23] H. Pérez-Acebo, A. Linares-Unamunzaga, R. Abejón, and E. Roj´, "Research trends in pavement management during the first years of the 21st century: A bibliometric analysis during the 2000–2013 period," *Applied Sciences*, vol. 8, no. 7, p. 1041, 2018.

[24] M. Treiber and D. Helbing, "An adaptive smoothing method for traffic state identification from incomplete information," in *Interface and Transport Dynamics*. Springer, 2003, pp. 343–360.

[25] T. Henning and D. Roux, "A probabilistic approach for modelling deterioration of asphalt surfaces," *Journal of the South African Institution of Civil Engineering*, vol. 54, no. 2, pp. 36–44, 2012.